Energetics and dynamics of unoccupied electronic states at the *h*-BN/Ni(111) interface

Matthias Muntwiler,* Matthias Hengsberger,† Andrei Dolocan, Hansjörg Neff, Thomas Greber, and Jürg Osterwalder
Universität Zürich, Physik-Institut, Winterthurerstrasse 190, CH-8057 Zürich, Switzerland
(Received 14 August 2006; revised manuscript received 24 October 2006; published 7 February 2007)

Adsorbed on the nickel (111) surface, hexagonal boron nitride (*h*-BN) forms a commensurate monolayer, which retains much of the band structure of layered bulk *h*-BN, specifically the wide band gap. This article explores its unoccupied band structure with femtosecond time-resolved two-photon photoelectron spectroscopy in a two-color setup, and presents spectra, dispersion, and cross-correlation measurements. Two distinct, dispersive intermediate states are observed at the origin of the surface Brillouin zone $\bar{\Gamma}$: a $\pi^\star$-related interface state at 1.51 eV above the Fermi level, which forms the conduction band, and an image-potential state at 0.65 eV below the vacuum level. With 260 fs for the image state and 110 fs for the interface state the lifetimes of the two unoccupied states are remarkably high due to the very small overlap of the corresponding wave functions with the nickel bulk states.

DOI: 10.1103/PhysRevB.75.075407 PACS number(s): 73.20.At, 73.40.Ns, 73.61.Ng, 78.47.+p

I. INTRODUCTION

Metal-insulator-metal (tunneling) junctions play a key role in electron and spin transport from applied as well as fundamental perspectives. Hexagonal boron nitride (*h*-BN) on a Ni(111) surface represents an ideal system for the study of such phenomena since *h*-BN forms an atomically sharp monolayer with a 1×1 superstructure and large domains.[1,2] The layer shows a simple band structure with a wide band gap and does not contribute electronic states at the Fermi level. For the case of C_{60}/*h*-BN/Ni(111) it has been demonstrated that the *h*-BN layer decouples the C_{60} molecules from the metallic substrate and enables a variable charging of the molecules based on molecular orientation.[3]

The atomic structure of the *h*-BN/Ni(111) interface is known in detail from various experiments[2,4,5] and calculations in density-functional theory (DFT).[6] As to the electronic band structure, the occupied σ and π bands found with angle-resolved ultraviolet photoemission spectroscopy (ARUPS) experiments[1] are well understood in terms of DFT calculations.[6] The unoccupied electronic structure, however, still remains controversial: Theoretically, Grad *et al.*[6] predict the conduction band at the $\bar{\Gamma}$ point at 1.5–1.7 eV above the Fermi level, which can be compared to the π-like interlayer state in bulk *h*-BN found by earlier LDA[7] and quasiparticle calculations.[8] At lower energies, the *h*-BN layer does not contribute to the unoccupied density of states. This picture has been confirmed by another DFT study by Che and Chen.[9] Previous experiments, however, do not agree: Using secondary electron spectroscopy, Nagashima *et al.* find the bottom of the conduction band 2.7 eV above the Fermi level,[1] whereas more recently from an x-ray-absorption study Preobrajenski and co-workers infer strong orbital hybridization between Ni 3*d* bands and *h*-BN π states.[10]

In this study, we probe the energetics and dynamics of unoccupied states of *h*-BN/Ni(111) with femtosecond time-resolved two-photon photoemission (TR-2PPE), which has become a well-established technique for this purpose.[11–13] By using short intense laser pulses to pump electrons from occupied to unoccupied states and to probe the transient population of the normally unoccupied state with a second photon, 2PPE combines the band-mapping capabilities of regular photoemission with the spectroscopy of unoccupied states. Specifically, the energy scale is easily referenced to the Fermi level, and angle scans allow one to map the dispersion up to about 0.5 Å^{-1} from $\bar{\Gamma}$, depending on the photon energy and the work function of the sample. Moreover, the electron dynamics, specifically the lifetimes of unoccupied states, can be studied in real time by varying the delay between pump and probe pulses. In particular, the study of long-lived image potential states with lifetimes in the range of tens up to several hundreds of femtoseconds by means of TR-2PPE constitutes one of the major successes of this method and allowed relaxation processes to be studied in great detail (see Ref. 14 and references therein).

II. EXPERIMENTAL

The *h*-BN/Ni(111) sample is prepared under ultrahigh vacuum (at a base pressure of 10^{-10} mbar) in a catalytic reaction of 50×10^{-6} mbar s of borazine $(HBNH)_3$ vapor with the hot Ni(111) surface at 1100 K according to the recipe by Nagashima *et al.*[15] The work function of the *h*-BN/Ni(111) samples was 3.6 eV [that of Ni(111) 5.37 eV] as measured with regular He I_α (21.22 eV) excited photoemission.

The analysis chamber is equipped with a hemispherical analyzer (VG ESCALAB 220), a two-axis goniometer for angle-scanned experiments,[16] and several x-ray sources and a microwave-driven He lamp for conventional photoelectron spectroscopy. The overall energy resolution (including laser) was 70 meV, and the angle resolution ±0.5°. A bias voltage of −10 V (unless otherwise stated) was applied to the sample in order to avoid the low-transmission region of the analyzer. All experiments were done at room temperature.

The laser pulses are generated by a commercial Ti:sapphire femtosecond laser (coherent Mira) with a tunable wavelength range of 790–850 nm, about 100 fs pulse length depending on the central wavelength, 0.5 W average power, and 76 MHz repetition rate. The pulses are frequency doubled in a 0.5-mm-thick β-barium borate (BBO) crystal, and the fundamental and second-harmonic beams are separated using dielectric mirrors. The fluence on the sample

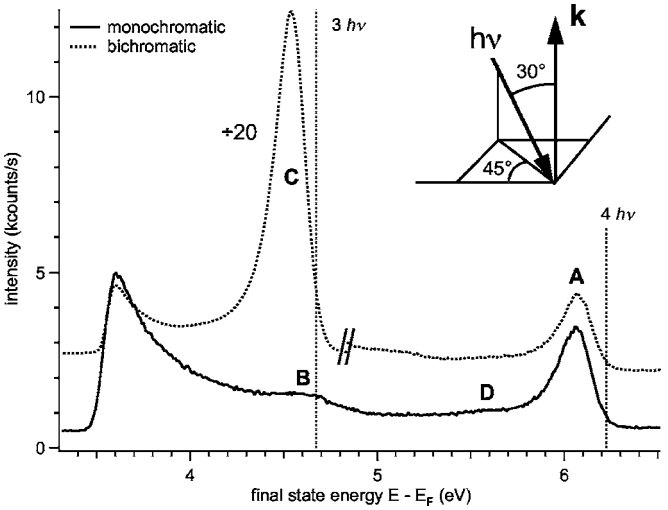

FIG. 1. 2PPE spectra of the *h*-BN/Ni(111) sample excited with 796 and 398 nm laser pulses. The monochromatic spectrum is measured using blue pulses only (the bichromatic using red and blue pulses in coincidence). The plots are vertically offset for better visibility, and the left-hand part of the bichromatic spectrum around the intense peak *C* is scaled down by a factor of 20. The energy scale refers to the energy of the final state (photoelectron) with respect to the Fermi level. The vertical lines indicate the final-state energies of the Fermi level as probed by a bichromatic ($3h\nu$) and a monochromatic ($4h\nu$) two-photon process, respectively. Inset: sketch of the geometry used; the light is impinging from behind at 30° with respect to the detector axis **k** and at 45° with respect to the manipulator axis; the polarization vector lies in the plane of incidence (*p* polarization).

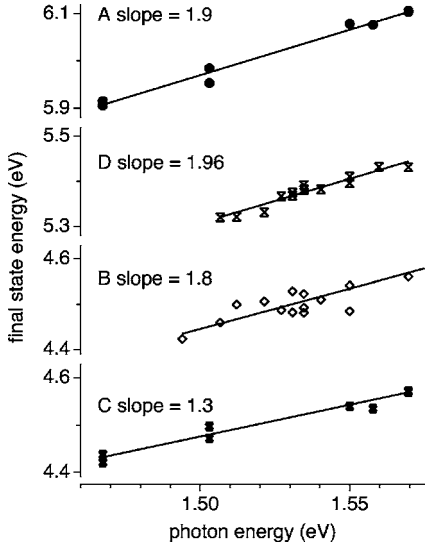

FIG. 2. Final-state energies of peaks $A-D$ versus fundamental (red) photon energy. Peaks *A*, *C*, and *D* are measured in both and peak *B* only in the monochromatic experiment. Slopes of 1 or 2 correspond to peaks of unoccupied states that are probed by a red or blue photon, respectively; slopes of 3 or 4 indicate occupied states.

typically was 35 μJ/cm^2 per pulse for the fundamental and 5 μJ/cm^2 for the second harmonic beam.

For *bichromatic* experiments both beams are used, while a computer-controlled translation stage varies the delay between the pulses of the two beams. Cross-correlation curves are obtained by recording the photoelectron intensity as a function of this pump-probe delay. The width of the instrument function, i.e., the experimental temporal resolution of combined red and blue pulses, was found to be 245 fs at 796 nm by recording transients from a nonresonant transition at the Fermi level on *h*-BN/Ni(111) or on polycrystalline silver.[17] Over the whole tunable range of the oscillator, the width of the cross-correlation profile of fundamental and second-harmonic increases from 165 fs at 845 nm to 273 fs at 790 nm.

In *monochromatic* experiments only one of the beams reaches the sample, and both pump and probe steps occur within the same laser pulse. As can be seen in the inset of Fig. 1 the direction of the light and that of the detector include an angle of 30°. Due to a nonorthogonal reflection on the last mirror, the light was not purely *p* polarized but contained an admixture of about 3% of *s*-polarized light. During all experiments the *h*-BN films showed no signs of radiation-induced damage.

III. RESULTS

Monochromatic and bichromatic 2PPE spectra excited with 796 nm (1.557 eV, "red") and 398 nm (3.116 eV, "blue") laser pulses measured at normal emission angle exhibit several clear peaks as displayed in Fig. 1. All these peaks must involve two-photon processes since the work function of the sample (3.6 eV) is higher than the photon energy of the second harmonic (3.1 eV). For peaks *A*, *B*, and *D*, both pump and probe photons must be blue ones because the peaks appear in the monochromatic spectrum. Due to the slope of ≈ 2 in the plot of final-state energy versus fundamental photon energy in Fig. 2, these peaks clearly bear the signature of unoccupied states, i.e., the energy of the final state is defined by the unoccupied state and the energy of the probe photon only. In contrast, the direct two-photon excitation process does not involve a real intermediate state of the sample, and the corresponding peak shifts with the total (pump and probe) photon energy.

In the bichromatic experiments of Fig. 1, peak *A* is still visible at similar intensity because the blue photon flux is not changed. Peak *B*, however, is dominated by the huge peak *C*, which is found 100 meV lower in energy. The two peaks can, however, be separated again at higher polar emission angles (as can be seen in Fig. 4). For peak C, the slope of the peak position versus fundamental photon energy is 1.3 (Fig. 2), which means that the peak also originates from an unoccupied state. It is at first glance not clear whether the deviation of that value from 1 (which would indicate that the state is probed by a red photon) is significant or not. In fact, as it will be pointed out later on, the peak is composed of two competing excitation processes, one blue-red and one red-blue, which are in resonance at ≈ 810 nm fundamental wavelength. A resonant process would also explain the huge amplitude, which drops quickly at higher and lower wavelengths. However, as the focus of this article lies on the energetics and dynamics of the unoccupied states, a detailed discussion of the resonance will be the subject of a separate paper.[18]

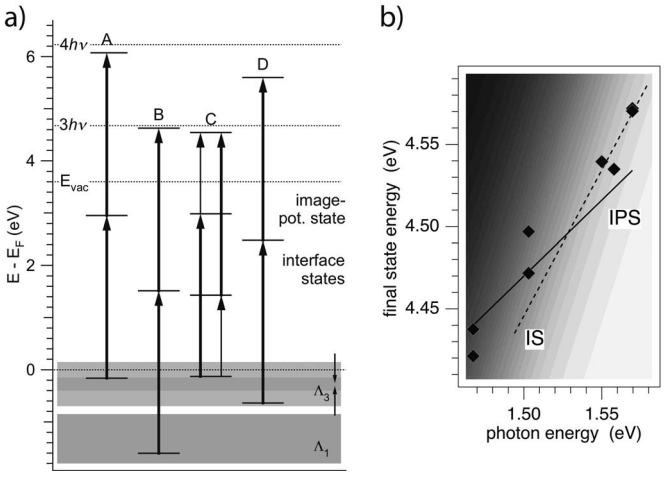

FIG. 3. (a) Schematic energy levels in normal emission with excitation paths deduced from the experimental results. Observed electronic states are marked with horizontal solid lines; states above the vacuum level E_{vac} correspond to free photoelectron final states. Vertical short and long arrows indicate transitions at 796 and 398 nm wavelength, respectively. The initial states for all observed peaks lie in the Λ_1 and Λ_3 bulk *d* bands of nickel, the bandwidths of which in $k_\perp$ are indicated by the shaded areas; the *h*-BN valence bands are not within reach of the experiment. (b) Final-state energies calculated from the energy levels for successive absorption of a red and a blue photon using the interface state as intermediate state (dashed line, IS) versus fundamental photon energy; the solid line IPS denotes the same for a blue-red process via the image-potential state; the diamonds denote the position of peak *C*. The gray scale of the background is proportional to the occupation factors of the initial states (Fermi-Dirac distribution; see text for details); white corresponds to a high number of occupied initial states.

Based on the spectroscopic information and its interpretation found so far, the energies of the involved states can be calculated. They are plotted schematically in Fig. 3. As will be argued in the discussion section, peak *A* at 2.95 eV above the Fermi level, i.e., at a binding energy of 0.65 eV with respect to the vacuum level, is assigned to an image-potential state, and peak *B* is assigned to the $\pi^\star$-derived conduction band of *h*-BN, 1.51 eV above the Fermi level.

The resonant process of peak *C* involves both the first interface state (*B*) and the image-potential state (*A*). This is visualized in the right panel of Fig. 3, where the final-state energy of the two possible intermediate states are plotted against the fundamental photon energy. As expected from excitations out of intermediate states, which require a red (IPS) or a blue (IS) photon as probe photon, the peak positions move with once and twice the fundamental photon energy, respectively. The color of the background scales with the Fermi-Dirac distribution convolved with a Gaussian in order to account for the finite experimental energy resolution. It represents the thermal occupation of the initial states involved. The experimental data points for peak *C*, which were added for comparison, roughly follow the two lines with an intermediate slope. As can be seen in the graph, starting from a common initial state, both excitation pathways end up at the same final state for a photon energy of about 1.53 eV (λ=810 nm). It is noted in passing that both, pump and probe photons need to be *p* polarized for peaks *A* and *C* to be observed. For this type of light polarization excitations out of Λ_1 and Λ_3 are possible. Since the direction of light incidence is fixed with respect to the detector (the inset of Fig. 1), the orientation of the electric field with respect to the surface normal is changed when the sample is rotated. As can be seen from Fig. 4(a), the photoemission intensity is higher for negative emission angles, i.e., when

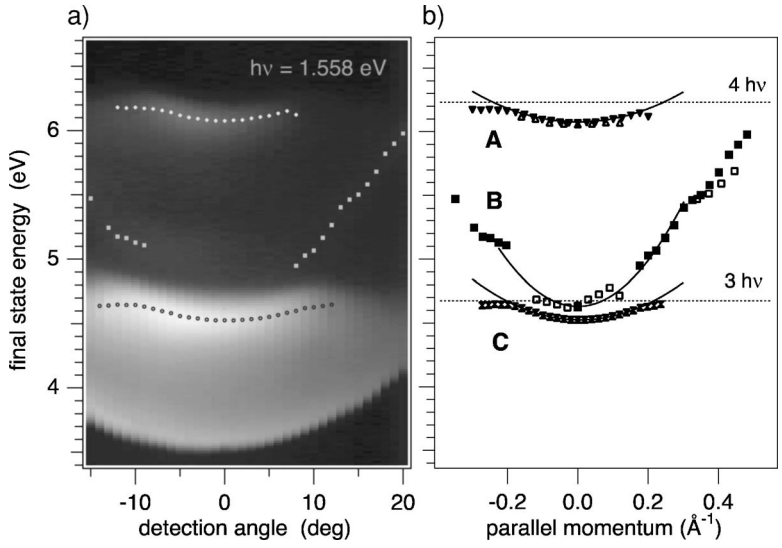

FIG. 4. Band map along $\overline{\Gamma M}$ ($\overline{M}$ is at 1.46 Å^{-1}). (a) Raw data as a function of the detection angle on a logarithmic gray scale ($\log_{10} I$) measured with the bichromatic setup; red and blue pulses arrive at the same time on the sample. The positions of peaks are indicated by symbols. (b) Peak positions versus momentum in the surface plane; solid and open symbols denote data taken with both red and blue light and only with blue light, respectively. Most of the data taken with blue light only have been measured using a sample bias of −3 V. The upper boundaries of peaks *A* and *C* reflect the Fermi level in the initial state (dotted horizontal lines). Parabola fits (solid lines) of the peak positions are used to determine effective masses $m^\star/m_e$: for peaks *A*, *B*, and *C*, we obtain 1.43±0.2, 0.43±0.1, and 1.12±0.2, respectively.

the sample is rotated *away* from the light source. In this case the field component perpendicular to the surface increases with increasing emission angle. Hence, we may conclude that the transition dipole is oriented perpendicular to the surface in agreement with previous studies of image-potential states (see Ref. 12, and references therein).

The dispersion measurement in Fig. 4(a) consists of a series of spectra at different polar emission angles in the $\overline{\Gamma M}$ azimuth. Two bright parabolic features corresponding to peaks *A* and *C*, and a weaker one corresponding to peak *B* can be found in the image. In order to calculate effective masses, peak positions (marked with circles) are determined from the raw spectral data by fitting Gaussian profiles. They are mapped to E versus $k_{\|}$ according to $\hbar k_{\|} = \sqrt{2m_e E_{\mathrm{kin}}} \sin\theta_x$, where E_{kin} denotes the kinetic energy of the electron in front of the sample surface and θ_x is the true emission angle [Fig. 4(b)]. The latter is obtained from the known angle between surface normal and detection direction θ_m taking into account the electrostatic field created by the bias voltage U between the sample and the entrance aperture of the analyzer:[19]

$$\theta_x = \theta_m + \arctan\left(\frac{eU(1-\sin\theta_m/\theta_m)}{E_{\mathrm{kin}} - eU(1-\sin\theta_m/\theta_m)}\right)^{1/2}.$$

Effective masses $m^\star$ are then obtained from the curvature of parabolic fits, so that $E = E_0 + \hbar^2 k_{\|}^2/(2m^\star)$. For peaks *A* and *C*, these fits are based on data points near the apex, where the proximity of the Fermi level in the initial state has a minimal effect on the peak shape. The dispersion of peak *B* deviates from a simple parabola, in particular, at momenta above ≈ 0.3 Å^{-1}, where the initial-state dispersion probably influences the peak dispersion. In order to stabilize the fit, the apex of the parabola was fixed at 4.63 eV, the value found in the blue-only spectrum of Fig. 1. With $m^\star \approx 0.43 \pm 0.1 m_e$ peak *B* significantly deviates from a free-electron-like behavior, whereas peak *C* exhibits an effective mass close to m_e. In contrast to feature *C*, peak *A* disperses with an effective band mass of about $1.43 m_e$, a value significantly above the free-electron rest mass. In terms of the band parameters described above, no significant difference is found in the $\overline{\Gamma K}$ azimuth (data not shown).

The only peak in this experiment that depends on the delay between red and blue pulses is peak *C*. Cross-correlation curves have been measured at various wavelengths by varying the optical-path length of the red laser beam; they are displayed in Fig. 5. The intensity is averaged from a 200-meV-wide energy interval centered on the peak. While the curves at 796 nm (photon energy 1.558 eV) and 825 nm (1.503 eV) are almost symmetric, the ones at 790 nm (1.57 eV) and 845 nm (1.467 eV) show an exponential tail on the negative or positive side, respectively. These tails indicate transient populations of intermediate states with lifetimes in the order of the width of the laser pulses or longer. Where they appear at positive delays they originate from an intermediate state that is pumped by a red photon and probed by a blue photon. For negative delays the opposite (blue-red) sequence applies. This strengthens the interpretation that peak *C* consists of a superposition of two processes as indicated in Fig. 3. At positive delays the measurement reveals the population of the interface state (red-blue process), whereas at negative delays (blue-red process) it reveals the population of the image-potential state. At longer wavelength (845 nm curve), the blue-red process is obviously suppressed because the pump step to the image-potential state is out of resonance. At shorter wavelength (790 nm curve) the opposite holds true giving rise to a clear blue-red transient suppressing effects of the second excitation channel.

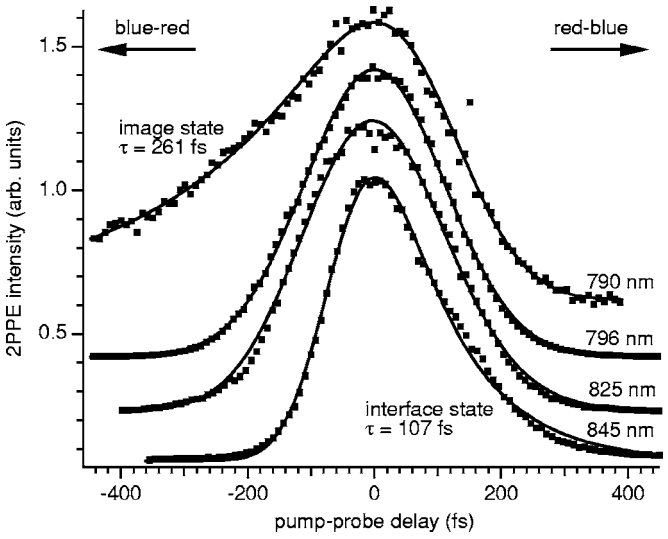

FIG. 5. 2PPE intensity of peak *C* as a function of pump-probe delay (cross correlation) at various wavelengths. The data points are averages over a 200 meV energy interval centered on the peak position at zero delay. The curves have been normalized since the peak amplitudes vary considerably, and their delay origin has been shifted to the maximum of the peak for convenience. Positive delays correspond to a red pump and blue probe (where the red pulse arrives before the blue one). The fit functions (lines) for the 790 and 845 nm data are based on the rate-equation model described in the text. For the 796 and 825 nm data they are simple Gaussians.

For a quantitative estimate of the lifetimes of the intermediate states the data are fit using a simple rate-equation model for a two-level system:[20]

$$\frac{dN_2}{dt}(t) = RI_{\mathrm{source}}(t) - \frac{N_2(t)}{\tau}, \tag{1}$$

where N_2 is the transient population of the intermediate state, R is an experimental fit parameter that contains the cross section and light intensity, I_{source} is the temporal intensity profile of the pump pulse, which we assume to be a Gaussian, and τ is the lifetime of the intermediate state. In general, the thus-obtained curve for N_2 would have to be convolved with the intensity profile of the probe pulse, also assumed to be Gaussian, in order to yield the measured transient curve. However, with such a convolution the widths of the pump and probe pulses would be treated as free parameters rendering the fitting process less stable. Good convergence is achieved by simply fitting N_2 of Eq. (1) using the cross-correlation profile as a source term. We checked using model pulse shapes and identical intermediate-state lifetimes that

both procedures led to results, which can hardly be distinguished.

Moreover, due to the low fluence employed in our experiments, saturation effects can safely be neglected. The model fits well to the image-potential state data at 790 nm, with a resulting lifetime of 261 fs. For the interface state, with a slightly worse fit, the lifetime is 107 fs. The error bars are estimated to be of the order of 10 fs. Notice that the two values have been derived from experiments at different wavelengths because it is hardly possible to extract lifetimes from measurements between 800 and 830 nm where the two channels apparently are resonating: the high intensity (Fig. 1) covers all other features and causes the transients of the peak to appear almost symmetric. The full width at half maximum of the simple Gaussians fitted to the transients taken with light of 796 and 825 nm wavelength amounts to 258 and 266 fs, respectively, thus slightly larger than the respective cross-correlation width given in Sec. II. At this stage we may only conjecture that the resonance process itself strongly distorts the transients as we do not observe any lifetime-related asymmetry in the data taken at resonance.[18]

IV. DISCUSSION

It is natural to assign the two peaks *A* and *B* that are visible in the monochromatic spectrum (Fig. 1) to two different intermediate states. These states must be surface states, image-potential states, or *h*-BN-induced states since bulk Ni has no states in this region of reciprocal space.[21] The energy at the band bottom at $\bar{\Gamma}$ (1.51 eV) and the dispersion ($m^\star = 0.43 m_e$) of peak *B* closely match the $E - E_F = 1.5, \ldots, 1.8$ eV and $m^\star \approx 0.73 m_e$ of the interface state predicted by Grad *et al.*[6]

Due to its energetic position 0.65 eV below the vacuum level, peak *A* is likely to be an image-potential state. Such states have been observed on various metal surfaces including clean Ni(111),[21,22] and they may persist in the presence of adsorbates.[23] The binding energy with respect to the vacuum level was found to be 0.8 eV for the bare Ni surface[21] close to the upper edge of the wide band gap at $\bar{\Gamma}$, which roughly extends from the Fermi level up to 6 eV above the Fermi level. Due to the strongly reduced work function in the case of *h*-BN/Ni(111) the image-potential state should shift downward by 1.8 eV towards the center of the bulk band gap. At the same time, the surface-potential barrier is changed by the presence of the *h*-BN monolayer and, as a consequence, the wave function moves away from the nickel surface plane. Wave functions of image-potential states have successfully been calculated for thin dielectric layers on metal surfaces. The corresponding binding-energy shifts reported for the case of a single dielectric monolayer were found to be of the order of 100 meV,[24] in agreement with our experimental observation. The effective mass of 1.43 in units of the free-electron rest mass, however, is significantly higher than the expected value of 1. Several models were proposed and rejected to explain the deviations of inverse photoemission results from the free-electron value (see Ref. 25 for a review), but neither surface corrugation nor proximity to the gap edges may explain our findings. Strong dipolar fields, which are present in the *h*-BN layer,[6] could influence the dispersion of the two-dimensional electron gas in front of the surface[26] but this interpretation requires further theoretical calculations.

With 261 fs the lifetime of the state is considerably higher than the 7 fs measured on the bare Ni(111) surface,[27] and also compared to the generally low lifetimes of unoccupied states in the proximity of a metal with an open *d* shell.[28] To a large extent such an increase can, again, be explained by the fact that the image-potential state is further away from the upper edge of the projected bulk band gap and that the center of gravity of its wave function is pushed away from the metal.[14] This decreases the overlap of the wave function with bulk states and thus reduces the scattering probability. Similar findings were reported from noble gas[29] and alkane[24] layers on various metal surfaces. The lifetime of the $n=1$ image-potential states typically increase by about an order of magnitude after adsorption of one monolayer of the dielectric due to the wave function being pushed away from the metal by the polarization of the dielectric. It is interesting to note that, as in the case of Xe,[29] the electron affinity of *h*-BN is attractive and would actually allow the electron wave function to penetrate the *h*-BN layer. The same reasoning could also hold for the lifetime of the interface state, which also lies within the band gap. Calculations, however, showed that the wave function is essentially localized between the metal surface and the *h*-BN-layer,[6] in agreement with previous calculations of bulk *h*-BN.[8]

The origin of peak *D* is less clear. Early density-functional[7] and many-body[8] calculations predicted a series of interlayer states for bulk hexagonal boron nitride. Such states persist in the limit of a single layer[8] and disperse in a free-electron-like fashion with a minimum at $\bar{\Gamma}$. Such states have been found for graphite using inverse photoemission,[30] and peaks *B* and *D* are likely to be the energetically lowest states of this series in the *h*-BN/Ni(111) system.

The composite nature of peak *C* needs some detailed attention. Based on energy levels as explained in the level diagram in Fig. 3, two excitation channels may contribute because the energy difference of 1.44 eV between the interface and image states is close to the fundamental photon energy: a red-blue channel probes the interface state while a blue-red channel probes the image state. We have already seen the contributions of either channel in the correlation curves of Fig. 5 if the photon wavelength is tuned out of resonance. In the spectra, the two states are not resolved within the photon-energy range accessible in our experiment ($1.47, \ldots, 1.57$ eV). The energy position of *C* is close to the value of the image-potential state probed with a red photon, but deviates from the position of the interface state as inferred from the blue-only experiments by about 100 meV. Moreover, the effective mass obtained for peak *C* lies between the values of the intermediate states contributing to the resonance. There are several possibilities for explaining the discrepancy in energy between the red-blue and blue-blue excitation paths via the interface state.

First, the initial-state bands differ for the two processes. For peak *B* ($E_i - E_F = -1.60$ eV) the electrons originate from the Λ_1 band, and for peak *C* ($E_i - E_F = -0.13$ eV) from the Λ_3

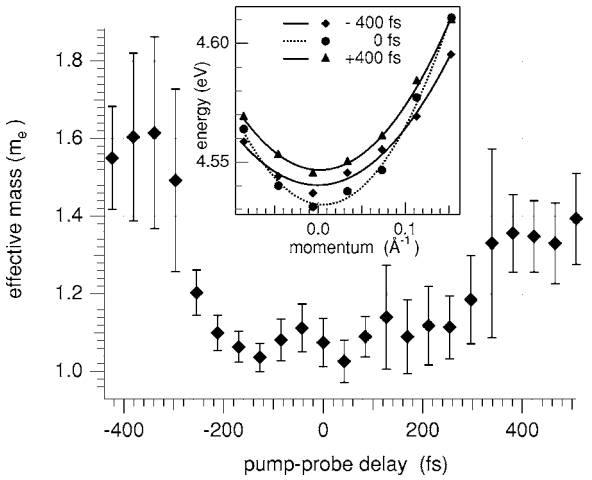

FIG. 6. Effective mass of peak C as a function of pump-probe delay. These values are calculated from a series of measured spectra at various pump-probe delays and at seven different angles around normal emission. Error bars indicate the standard deviation of the fit parameters (of the Gaussian peak position and parabolic-dispersion fits) based on the analysis of the χ^2 function. Inset: dispersion around $\bar{\Gamma}$ along $\bar{\Gamma}M$ for three different time delays (−400 fs, 0 fs, +400 fs). The measurements have been taken in resonance with a fundamental of 796 nm wavelength.

band, which both are part of the high-density, exchange-split $3d$ band system of bulk nickel.[31,32] Thus, the peak may shift due to the specific momentum and energy of the initial states. Still considering the two different initial-state bands, a second possible explanation arises from a magnetic-exchange splitting in the interface state induced by the nickel substrate as predicted by theoretical calculations (splitting of 120 meV at $\bar{\Gamma}$, Ref. 6). Put in another way, the peaks observed as peak B in red-blue and blue-blue experiments may be of different spin character, the one closer to the optical-resonance condition dominating the spectrum. A third scenario for the 100 meV peak shift may invoke the formation of polarons in the highly polar boron-nitride lattice.[33,34] However, we do not observe the effects that are common manifestations of localization processes, such as increasing binding energy and increasing effective mass over a time scale of a few to a few hundred femtoseconds.[35] Although we do observe a variation of effective mass with pump-probe delay as shown in Fig. 6, this change is small; $m^\star/m_e$ decreases close to zero ruling out the possibility of fast localization processes. Finally, the excitation mechanism of the resonance itself may lead to a transient change in dispersion. As can be seen in Fig. 6, the effective mass changes over a time scale which matches the width of the cross-correlation function in resonance (Fig. 5). However, the excitation mechanism needs some further investigation, and a final explanation of the transient effective mass is still missing.[36]

V. CONCLUSIONS

In two-photon photoemission spectra of monolayer h-BN on Ni(111) we find the signatures of an image-potential state 0.65 eV below the vacuum level and of an interface state 1.51 eV above the Fermi level. The interface state fits well into the theoretical picture by Grad *et al.*[6] With reference to earlier photoemission experiments[1,6] we find an experimental value of 6.0 eV for the indirect π-$\pi^\star$ photoemission gap of the h-BN layer as adsorbed on Ni(111). The direct σ-$\pi^\star$ photoemission gap at the center of the Brillouin zone $\bar{\Gamma}$ amounts to 6.8 eV. The enhanced lifetimes of the two unoccupied states (261 fs for the image-potential state and 107 fs for the interface state) reflect the presence of the projected L gap of the bulk band structure of nickel. While the long lifetime of the image-potential state can be taken as a consequence of the h-BN-spacer layer, the lifetime of the interface state in close proximity to the surface of a metal with an open d shell is astonishingly long.

ACKNOWLEDGMENTS

The authors would like to thank P. Hamm, C. D. Lindstrom, and X.-Y. Zhu for valuable discussions, H. Sachdev for providing borazine, and C. Cirelli for assistance with the laser setup. This work has been supported by the Swiss National Science Foundation.

*Present address: University of Minnesota, Department of Chemistry, 207 Pleasant St. SE, Minneapolis, MN 55455, USA. Electronic address: muntwiler@chem.umn.edu

†Corresponding author. Electronic address: matthias@physik.unizh.ch

[1] A. Nagashima, N. Tejima, Y. Gamou, T. Kawai, and C. Oshima, Phys. Rev. Lett. **75**, 3918 (1995).

[2] W. Auwärter, T. J. Kreutz, T. Greber, and J. Osterwalder, Surf. Sci. **429**, 229 (1999).

[3] M. Muntwiler, W. Auwärter, A. P. Seitsonen, J. Osterwalder, and T. Greber, Phys. Rev. B **71**, 121402(R) (2005); URL http://dx.doi.org/10.1103/PhysRevB.71.121402

[4] Y. Gamou, M. Terai, A. Nagashima, and C. Oshima, Sci. Rep. Res. Inst. Tohoku Univ. A **44**, 211 (1997).

[5] M. Muntwiler, W. Auwärter, F. Baumberger, M. Hoesch, T. Greber, and J. Osterwalder, Surf. Sci. **472**, 125 (2001); URL http://dx.doi.org/10.1016/S0039-6028(00)00928-6

[6] G. B. Grad, P. Blaha, K. Schwarz, W. Auwärter, and T. Greber, Phys. Rev. B **68**, 085404 (2003); URL http://dx.doi.org/10.1103/PhysRevB.68.085404

[7] A. Catellani, M. Posternak, A. Baldereschi, and A. J. Freeman, Phys. Rev. B **36**, 6105 (1985); URL http://dx.doi.org/10.1103/PhysRevB.32.6105

[8] X. Blase, A. Rubio, S. G. Louie, and M. L. Cohen, Phys. Rev. B **51**, 6868 (1995); URL http://dx.doi.org/10.1103/PhysRevB.51.6868

[9] J. G. Che and H.-P. Cheng, Phys. Rev. B **72**, 115436 (2005); URL http://dx.doi.org/10.1103/PhysRevB.72.115436

[10] A. B. Preobrajenski, A. S. Vinogradov, and N. Mårtensson, Phys. Rev. B **70**, 165404 (2004).
[11] T. Fauster and W. Steinmann, in *Electromagnetic Waves: Recent Developments in Research* (Elsevier Science, Amsterdam, 1995), Vol. 2, p. 347, Chap. 8.
[12] M. Wolf, A. Hotzel, E. Knoesel, and D. Velic, Phys. Rev. B **59**, 5926 (1999).
[13] U. Höfer, I. L. Shumay, Ch. Reuß, U. Thomann, W. Wallauer, and Th. Fauster, Science **277**, 1480 (1997).
[14] P. M. Echenique, R. Berndt, E. V. Chulkov, T. Fauster, A. Goldmann, and U. Höfer, Surf. Sci. Rep. **52**, 219 (2004).
[15] A. Nagashima, N. Tejima, Y. Gamou, T. Kawai, and C. Oshima, Phys. Rev. B **51**, 4606 (1995).
[16] T. Greber, O. Raetzo, T. J. Kreutz, P. Schwaller, W. Deichmann, E. Wetli, and J. Osterwalder, Rev. Sci. Instrum. **68**, 4549 (1997).
[17] T. Hertel, E. Knoesel, M. Wolf, and G. Ertl, Phys. Rev. Lett. **76**, 535 (1996).
[18] M. Hengsberger, M. Muntwiler, T. Greber, and J. Osterwalder (unpublished).
[19] It is not trivial to determine the true $k_{\|}$ scale because the bias voltage of the sample creates an electrostatic lens with the entrance of the analyzer. A model of ballistic electron flight between two oblique plates was used; details will be published elsewhere. The agreement between the different data sets in Fig. 4 taken at different bias voltages is good indicating that the assumed model works well for emission angles below 30°.
[20] C. D. Lindstrom, D. Quinn, and X.-Y. Zhu, J. Chem. Phys. **122**, 124714 (2005).
[21] S. Schuppler, N. Fischer, W. Steinmann, R. Schneider, and E. Bertel, Phys. Rev. B **42**, 9403 (1990).
[22] A. Goldmann, M. Donath, W. Altmann, and V. Dose, Phys. Rev. B **32**, 837 (1985).
[23] D. F. Padowitz, W. R. Merry, R. E. Jordan, and C. B. Harris, Phys. Rev. Lett. **69**, 3583 (1992).
[24] R. L. Lingle, Jr., N.-H. Ge, R. E. Jordan, J. D. McNeill, and C. B. Harris, Chem. Phys. **205**, 191 (1996).
[25] N. V. Smith, Rep. Prog. Phys. **51**, 1227 (1988).
[26] G. Dutton, J. Pu, D. G. Truhlar, and X. Y. Zhu, J. Chem. Phys. **118**, 4337 (2003).
[27] S. Link, J. Sievers, H. A. Dürr, and W. Eberhardt, J. Electron Spectrosc. Relat. Phenom. **114-116**, 351 (2001).
[28] M. Aeschlimann, R. Burgermeister, S. Pawlik, M. Bauer, D. Oberli, and W. Weber, J. Electron Spectrosc. Relat. Phenom. **88-91**, 179 (1998).
[29] M. Wolf, E. Knoesel, and T. Hertel, Phys. Rev. B **54**, R5295 (1996).
[30] Th. Fauster, F. J. Himpsel, J. E. Fischer, and E. W. Plummer, Phys. Rev. Lett. **51**, 430 (1983).
[31] D. E. Eastman, F. J. Himpsel, and J. A. Knapp, Phys. Rev. Lett. **40**, 1514 (1978).
[32] K.-P. Kämper, W. Schmitt, and G. Güntherodt, Phys. Rev. B **42**, 10696 (1990).
[33] E. Rokuta, Y. Hasegawa, K. Suzuki, Y. Gamou, C. Oshima, and A. Nagashima, Phys. Rev. Lett. **79**, 4609 (1997).
[34] A. A. Pavlychev, R. Franke, S. Bender, and J. Hormes, J. Phys.: Condens. Matter **10**, 2181 (1998).
[35] N.-H. Ge, C. M. Wong, R. L. Lingle, Jr., J. D. McNeill, K. J. Gaffney, and C. B. Harris, Science **279**, 202 (1998).
[36] It was checked that the maximum total-electron yield corresponds to emission rates of less than one electron per pulse; Coulomb repulsion between simultaneously emitted electrons can therefore be excluded as explanation for the transient change in effective mass close to the maximum of the resonance.